OpenNano 9 (2023) 100116

Contents lists available at ScienceDirect

OpenNano

journal homepage: www.elsevier.com/locate/onano

Characterization of glioblastoma spheroid models for drug screening and phototherapy assays

Samara Rodrigues Alves [a,1], Italo Rodrigo Calori [a,1], Hong Bi [b], Antonio Claudio Tedesco [a,c,*]

[a] Department of Chemistry, Center of Nanotechnology and Tissue Engineering- Photobiology and Photomedicine Research Group, Faculty of Philosophy, Sciences and Letters of Ribeirão Preto, University of São Paulo, São Paulo, Ribeirão Preto 14040-901, Brazil
[b] School of Materials Science and Engineering, Anhui University, Hefei 230601, China
[c] School of Chemistry and Chemical Engineering, Anhui Key Laboratory of Modern Biomanufacturing, Anhui University, Hefei 230601, China

ARTICLE INFO

Keywords:
Glioblastoma
Multicellular tumor spheroid
3D cell model
Nanoparticles
Photodynamic therapy

ABSTRACT

Glioblastoma (GBM) spheroids present as a promising alternative testing platform for *in vivo* models of brain cancer, aiming at the 3Rs principle of animal use in pre-clinical trials. However, the poor characterization and irreproducibility of various GBM-based spheroids have hampered the achievement of statistically relevant data for drug screening and photodynamic therapy (PDT) assays. In a previous study (Calori et al., 2022), we defined the conditions for inducing tight compaction of U87MG, T98G, UW473, A172, and U251 GBM cell lines into reproducible 3D spheroids using type I collagen as an extracellular matrix. Herein, GBM spheroids were characterized in their growth profile, proliferation rate, cell viability, necrotic nucleus, and cell death mechanisms and applied in PDT assays. Driven by proliferation, U87MG and A172 spheroids grew with time, at least up to day 12, whereas T98G and U251 demonstrated little change. The order of cell viability of spheroids over time was U87MG > A172 > U251 > T98G. A necrotic nucleus was formed over time for all cell lines, as shown by histological assays and the inverse size-cell viability relationship. When subjected to PDT, all spheroids showed a dose-dependent response, with an excellent dose-light-cell viability correlation. The higher light dose required for PDT of GBM 3D spheroids compared with the simplest 2D monolayers and its proximity to *in vivo* dose response in the literature is proof of its applicability in pre-clinical tests to reduce the use of animals in research.

1. Introduction

The number of pathways for the development of new drugs and clinical procedures requires time and different phases before reaching the final goal in human history. Recently, phases 1, 2, and 3 have become familiar terms and procedures discussed in the community. Subsequently, clinical trials in animals, following ethical protocols, have been used in pre-clinical assays of drug development and are often accepted as ethically appropriate to predict toxicity, efficacy, mechanisms of action, pharmacokinetics, and

* Corresponding author at: Department of Chemistry, Center of Nanotechnology and Tissue Engineering- Photobiology and Photomedicine Research Group, Faculty of Philosophy, Sciences and Letters of Ribeirão Preto, University of São Paulo, São Paulo, Ribeirão Preto 14040-901, Brazil.
E-mail address: atedesco@usp.br (A.C. Tedesco).
[1] These authors contributed equally to this work.

https://doi.org/10.1016/j.onano.2022.100116
Received 27 September 2022; Received in revised form 29 November 2022; Accepted 13 December 2022
Available online 14 December 2022

pharmacodynamics [1,2]. However, in the 20th and 21st centuries, the use of animals in research has sometimes been widespread, unconscious, and severe [3]. Only in the United States, it is estimated that 111.5 million rats and mice were used in a year for scientific research between 2017 and 2018, where approximately 44.5 million of these animals were potentially submitted to painful experiments [4]. Although widely used, animal models, such as human surrogates, can largely fail to predict human toxicology and drug safety [5–7]. In some cases, *in vitro* models are better at predicting human drug hazards than animal (or human) studies [8]. Based on this, along with the 3Rs principles for the replacement, refinement, and reduction of animals, a normative protocol began to be used in pre-clinical studies since the original definition of Russell and Burch [9]. Even when developed in a controlled manner, there are clear indications that the scientific community must develop animal substitute models that closely resemble human complexity [10].

In oncology, monolayer (2D) cell cultures have been widely used to assess drug activity [11]. However, its 2D architecture limits its physiological relevance, leading to divergent findings compared with *in vivo* results. 3D culture models, such as multicellular tumor spheroids (MCTS), which have been exponentially growing in studies, are considered promising physiological models for the *in vivo* microenvironment of solid tumors for cancer studies [12].

MCTS are cell aggregates that are compacted into sphere-like arrangements. MCTS produced with cancer cells presents an intermediate complexity between the commonly used 2D cultures and *in vivo* 3D environments. Owing to the 3D structure and compaction of spheroids, MCTS closely mimic the characteristics of solid tumors, including heterogeneous structural organization, cell-to-cell and cell-to-extracellular matrix interactions, growth kinetics, internal gradients of nutrients and oxygenation, and resistance to chemotherapy and radiotherapy.

Glioblastoma (GBM, a WHO grade IV tumor) is the most aggressive intracranial tumor in adults, accounting for 48.6% of all malignant central nervous system tumors [13]. GBM is highly infiltrative, recurrent, treatment-resistant, and has a poor prognosis. The 5-year survival rate of GBM patients is 6.8%, with an average length of survival of approximately 15 months. Moreover, the incidence of GBM has risen from 0.59 to approximately 4 per 100,000 population from 2008 to 2017 [14,15]. However, no significantly advanced statistics have been obtained in recent decades [16]. Besides being one of the most expensive cancers to treat, the only five drugs approved by the FDA have not significantly extended patient lives over a few months [16].

Spheroids have been used to track the evolution of GBM, elucidate resistance mechanisms, and propose novel therapy strategies [17–19]. A recent study showed that a 3D model of GBM demonstrated more resistance to Temozolomide, the gold standard drug for GBM chemotherapy [20]. The authors also found that resistance was potentialized by hypoxia, in which assays using 3D models contributed to finding strategies to overcome resistance to treatment. Another recent study explored the 3D architecture of GBM spheroids to evaluate the deep translocation of nanoscale drug delivery systems in GBM [21], which is impossible using 2D models. Nevertheless, just a few studies used 3D spheroids for drug screening and photodynamic therapy (PDT) assays.

PDT is a clinical protocol that uses photosensitizer (PS) molecules, molecular oxygen, and visible light to generate reactive oxygen species (ROS) *in situ,* causing cell death [22]. In addition to the promising results of PDT as an adjuvant therapy to treat GBM [23–25], a large number of parameters, including PS concentration, accumulation time, light dose, and light penetration [22] require an excessive number of animals to optimize the therapeutic response in pre-clinical assays. Alternative in vitro models that are efficient in mimic the in vivo microenvironment might be useful to reduce and replace the animal use in research studies, which agree with the 3R's principle [26]. In this scenario, while 2D monolayers are ineffective models to mimic the oxygen gradient in solid tumors, tumor spheroids come close to that condition typically due to the cell's growth in three dimensions in a compacted form. Thus, tumor spheroids have been applied in studies of complex PDT protocols such as combined therapies using PDT and radiotherapy, hyperthermia, chemotherapy as well as metronomic PDT with the study of the effects of power irradiance on the effectiveness of PDT [27] and penetration of photossensitizers [28], Moreover, tumor spheroids permit to monitor the effects of treatment directly in the cells without any lateral influence such as the effect of the tumor vasculature, immunological reactions, and others impacts related to the in vivo environment [29].

In a recent study, we defined the conditions under which loose aggregates of GBM cells compact into tight, compact 3D spheroids in the presence of type I collagen [30]. Here, we characterized and compared GBM spheroids formed by U87MG, A172, U251, and T98G cell lines to provide detailed GBM spheroid models for drug and phototherapeutic screening in an easy-handling manner. GBM spheroids were evaluated for growth, viability, proliferation rate, cell death mechanisms, and histological development. We also evaluated the correlation between cell viability data from trypan blue and acid phosphatase to verify the applicability of acid phosphatase in predicting the viability of our spheroids in drug screening as a rapid routine analysis. Using PDT from aluminum chloride phthalocyanine-loaded liposomes (Lip-Pc), we evaluated the light dose needed for therapeutic response to validate our spheroids as a viable model for PDT assays aimed at reducing animal use in GBM therapy. This is the first time that collagen-containing spheroids from four GBM cell lines named U87MG, T98G, A172, and U251 are characterized and compared according to their viability, proliferation, volume and histology along with its use in PDT as a proof of its applicability in pre-clinical tests. It is worth noting that the acid phosphatase assay was demonstrated to be effective in cell viability assay for these GBM spheroids without the need for spheroid disintegration.

2. Materials & methods

2.1. Materials

Dulbecco's modified Eagle medium (DMEM), non-essential amino acids, amphotericin, penicillin, streptomycin, trypsin-EDTA, fetal bovine serum (FBS), and phosphate-buffered saline (PBS) were purchased from Life Technologies (Thermo Fisher Scientific Inc., Waltham, MA, USA). Accutase solution (400–500 units/mL) and 4-nitrophenyl phosphate tablets were purchased from Sigma-

Aldrich (St. Louis, MO, USA). Type-I collagen was purified from rat tail tendons as described previously [31]. A standard stock solution of 1.57 mg mL^{-1} collagen was prepared in acetic acid (20 mmol L^{-1}). Collagen-fluorescein (FITC) conjugate was purchased from BioVision (BioVision Inc., Milpitas, CA, USA). Lipid 1,2-dimyristoyl-sn-glycero-3-phosphatidylcholine (DMPC) was purchased from Avanti Polar Lipids Inc. (Birmingham, AL, USA). All PBS solutions (pH 7.4) were prepared at final concentrations of 10 mmol L^{-1} phosphate, 137 mmol L^{-1} NaCl, and 2.7 mmol L^{-1} KCl. Ultrapure water (Milli-Q) was used in all the experiments.

2.2. Instruments

The cell plates were centrifuged using an Eppendorf 5810R- Benchtop Centrifuge (Eppendorf SE, Hamburg, HH, DE). Absorbance values were obtained using a Cytation 5 Cell Imaging Multi-Mode Reader (BioTek, Winooski, VT, USA) with an excitation wavelength of 404 nm and a baseline of 650 nm. Optical images were acquired using an optical microscope Carl Zeiss Microscopy with 5 × and 10 × objectives coupled to a ZEISS Axiocam Microscope Camera (Carl Zeiss NTS Ltd., Oberkochen, BW, DE). Confocal laser scanning microscopy was performed using a Leica TCS-SP8 confocal laser scanning microscope (Leica Microsystems, Wetzlar, Germany). Flow cytometry data were acquired using a Guava easy Cyte 8HT benchtop flow cytometer (Guava Technologies, Hayward, CA, USA). Data analyses were performed using Guava CytoSoft 4.2.1 Software and FlowJo Version 10 software. The hydrodynamic diameter (H_D) and polydispersity index (PDI) of the liposomes were determined by dynamic light scattering (DLS) using a Nano ZetaSizer (Malvern Panalytical Ltd, Malvern, WORCS, UK). Spheroids were irradiated using a 660 nm LED BOX (biolambda, São Paulo, SP, Brazil).

2.3. Cell culture

U87MG, T98G, U251, and A172 cell lines were acquired from the American Type Culture Collection (ATCC, Manassas, VA, USA) and cultured in T75 flasks for adherent cells in DMEM supplemented with 10% FBS, 100 U mL^{-1} penicillin, 100 mg mL^{-1} streptomycin, 250 ng mL^{-1} amphotericin B, and 0.1 mmol L^{-1} MEM non-essential amino acids. Cell lines were grown in an incubator at 37°C in a humidified atmosphere of 5% CO_2. Cell detachment for cell passage was performed using PBS solution (pH 7.4, 10 mmol L^{-1}) containing 0.05% trypsin and 0.02% EDTA.

2.4. MCTS formation

MCTS were prepared as previously described [30]. In summary, 100 μL of cell suspension (from 0.89×10^4 to 5×10^4 cells mL^{-1} in 1 × DMEM 10% FBS) was added to each well of an ultra-low attachment (ULA) 96-well round-bottom plate (Corning Inc., New York, NY, USA). After centrifugation (300 *g*, 3 min), the plate was incubated at 37 °C for 24 h. Subsequently, 100 μL of a colloidal type-I collagen solution (40.0 mg mL^{-1}, DMEM 15% FBS) was added to each U87MG, A172, and T98G cell line well spheroids. The plate was centrifugated (100 *g*, 1 min). For U251, the same procedure was applied, but using a collagen-free DMEM 15% FBS. The plates were incubated at 37°C for the time required for each experiment. Half of the culture medium was renewed every each three days using a fresh 1 × DMEM 15% FBS.

2.5. Growth and morphology of spheroids

ImageJ software was used to determine spheroid growth, morphology, and average radius (r) from optical images. The spheroid surface area (A) was estimated using the following formula: $A = \pi \times r^2$.

2.6. Cell viability using acid phosphatase

The cell viability of spheroids was determined based on a previously described method [30,32]. Spheroids were washed twice by transferring 50 μL of the culture medium containing spheroids to a novel well of a 96-well flat-bottom plate, followed by the addition of 150 μL PBS (pH 7.4, 10 mmol L^{-1}). Further, 100 μL of the solution containing the spheroids was transferred to another well followed by 100 μL of acid phosphatase solution (1.8 mg mL^{-1}). The plates were then incubated for 90 min at 37°C. Ten microliters of NaOH solution (1.0 mol L^{-1}) were added to each well and the plate was incubated for 20 min at room temperature (RT). After incubation, the absorbance at 405 nm and the baseline at 650 nm were recorded using a plate reader. Eight wells without spheroids were used to determine the blank values. A blank solution was used to correct the absorbance values.

2.7. Cell viability using trypan blue

The trypan blue assay was used to determine the viability of spheroids by counting viable cells. Briefly, eight spheroids (in 50 μL of culture medium each) were transferred to an Eppendorf tube (2 mL in volume). The spheroids were centrifuged (1400 rpm for 5 min), and the culture medium was removed. PBS (500 μL (pH 7.4, 10 mmol L^{-1}) was added, followed by centrifugation (1400 rpm for 5 min). The supernatant was removed and 250 μL of Accutase solution (400–500 units/mL) was added. After 30 min of incubation (with cell dispersion using a pipette every 10 min), 250 μL of FBS-free DMEM was added. The tubes were centrifuged (1400 rpm, 8 min), the supernatant was removed, and 100 μL trypan blue solution was added. Viable cells were counted using a Neubauer Chamber.

2.8. Flow cytometry

After the accutase protocol described in 2.7 using 24 spheroids (initial 2000 cells/spheroid, days 4 and 12), cells were resuspended in Nexin reagent +7AAD medium (50 μL reagent + 150 μL 1 × DMEM medium). The tubes were then incubated in the dark for 20 min. Flow cytometry was performed to obtain 5×10^3 cells per sample. Data were analyzed using the Guava CytoSoft 4.2.1 software.

2.9. Histochemistry (H&E)

Spheroids (2000 cells/spheroid, days 4 and 12) were fixed using 10% formaldehyde for 10 min at RT, placed in alcoholic eosin Y solution 1% (m/v), and washed in PBS (pH 7.4, 10 mmol L^{-1}). Spheroids were frozen in Tissue-Tek O.C.T. Serial sections (10 μm) were prepared using a cryostat (−16 °C). Sectioned samples were hydrated in a series of solutions as follows: 100, 90, 80, 70, and 50% ethanol: water (v/v) solution, stained with Hematoxylin and Eosin (H&E), hydrated using a series of ethanol: water solutions, clarified in xylene, and finished with Eukitt mounting medium.

2.10. Synthesis of Lip-Pc

Liposomes containing Aluminum Chloride phthalocyanine (AlClPc), named Lip-Pc, were prepared by ethanol injection [33]. A mass of 12.2 mg of DMPC was solubilized in 440 μL of an ethanolic solution containing 681.7 μmol L^{-1} AlClPc. The solution was injected into 30.0 mL of DMEM culture medium (37°C) at 1 μL/s.

2.11. Cell uptake and penetration range of Lip-Pc

The cellular uptake and penetration range of Lip-Pc were determined using steady-state fluorescence and confocal microscopy, respectively. U87MG spheroids (2000 cells/spheroid, day 4) were incubated with Lip-Pc (10 μmol L^{-1}) in DMEM (3% FBS) for 20 min, 1, 2, 4, and 6 h. Spheroids were washed twice with PBS (pH 7.4, 10 mmol L^{-1}). For cell uptake, seven spheroids in 10 μL of culture medium were transferred to a 1.5 mL Eppendorf tube at each time point. The tube was centrifuged (1400 rpm, 5 min), the supernatant was removed, and the spheroids were washed once in PBS (pH 7.4, 10 mmol L^{-1}) and centrifuged again. After removing the supernatant, 100 μL of trypsin (0.05%) was added and incubated for 20 min to promote the disintegration of spheroids. Isopropanol (200 μL) was added and incubated for 24 h at 4°C to extract Pc. The solutions were transferred to a 96-well plate and steady-state fluorescence were measured at 630 nm. For penetration range analysis, three spheroids at each time point were fixed using formaldehyde (10%) for 10 min, placed in eosin solution, and then in PBS solution (pH 7.4, 10 mmol L^{-1}). Spheroids were frozen in Tissue-Tek O.C.T. and serial sections (10 μm) were obtained using a cryostat. Slides containing spheroid sections were closed with glass coverslips containing the Fluoromount-G mounting medium. Confocal microscopy of sectioned spheroids was used to acquire images of AlClPc with excitation at 630 nm and an emission range between 660–750 nm.

2.12. Cytotoxicity of Lip-Pc

U87MG spheroids (initial 2000 cells/spheroid, day 4) were incubated with 0, 1.0, 2.0, 4.0, 7.0, and 10.0 μmol L^{-1} of AlClPc loaded in liposomes (culture medium supplemented with 3% FBS). After 4 h of incubation in the dark, the spheroids were washed twice in PBS (pH 7.4, 10 mmol L^{-1}) and incubated for 24 h at 37°C. The acid phosphatase method was used to determine cell viability, as described in Section 2.6.

2.13. Photodynamic therapy assays

Spheroids of GBM (initial 2000 cells/spheroid, day 4) were incubated with 10.0 μmol L^{-1} of AlClPc loaded in liposomes (DMEM medium supplemented with 3% FBS). After 4 h of incubation in the dark, the spheroids were washed twice with PBS (pH 7.4, 10 mmol L^{-1}). Spheroids were irradiated using a 660 nm LED light at 30 mW/cm^2 for 0.56 min (1 J/cm^2), 5.56 min (10 J/cm^2), 27.78 min (50 J/cm^2), and 55.56 min (100 J/cm^2) and incubated for 24 h at 37 °C. Cell viability was determined using the acid phosphatase method described in Section 2.6. The control groups were spheroids without Lip-Pc and light, spheroids without Lip-Pc and 100 J/cm^2, and spheroids with Lip-Pc (10 μmol L^{-1}) and without light.

2.14. Statistical analysis

GraphPad Prism 9 software was used for statistical data analysis (GraphPad Software, San Diego, CA, USA). Data were expressed as mean ± standard deviation. Statistical significance was determined by the Student t-test considering $p < 0.05$. All experiments were performed in triplicates with at least eight spheroids for each replicate.

3. Results and discussion

3.1. Growth and cell viability

To evaluate spheroid growth and viability as a function of time, we prepared U87MG, A172, and T98G spheroids (2000 cells per spheroid) according to our previous work [30] where loose cell aggregation was provided by centrifugation in an ultra-low attachment (ULA) round-bottom plate followed by tight compaction in the presence of type-I collagen ($[collagen]_{final}$ = 20 μg/mL). U251 spheroids were formed in the absence of collagen and used as a negative-collagen control, because of their ability to self-aggregate in compact spheroids.

The timeline of spheroid formation is illustrated in Fig. 1A. On day two, all spheroids had a similar mean diameter, ranging from 333 (±4) to 393 (±7) μm (Fig. 1B). (Fig. 1B). Conversely, they differ entirely as a function of time. U87MG spheroids grew as a linear function of time in volume (Fig. 1C) up to day 12, with a final mean diameter of 818 (±2) μm. A similar behavior was observed for the A172 spheroid, with a final mean diameter of 664 (±24) μm. The significant increase in both spheroids indicated that proliferative processes were present within the evaluated period.

Contrary to the U87MG and A172, the mean diameters of the U251 and T98G spheroids did not increase over time. A short decrease was observed for U251 from 333 (±4) to 305 (±3) μm from day 2 to day 12. These results suggested that the cell proliferation process was insignificant for U251 and T98G cells or that cell viability decreased faster than the proliferation time. To test these hypotheses, we verified the viability of spheroids by viable cell counting analysis using trypan blue assays (Fig. 1D). For the U87MG spheroids, cell viability increased from day 2 to day 8. After this period, cell viability started to decrease. Since the diameter of U87MG spheroids continues to increase after day 8, cell death processes must be most pronounced at the center of the spheroids.

However, cell proliferation continued in the interfacial region. These results suggested that a necrotic nucleus was formed on day eight. Because the mean diameter of the U87MG spheroids was 705 (±7) μm on day eight, this might be a key factor in the formation of necrotic nuclei. A similar behavior was seen for A172 spheroids, with cell viability increasing up to day eight and decreasing thereafter.

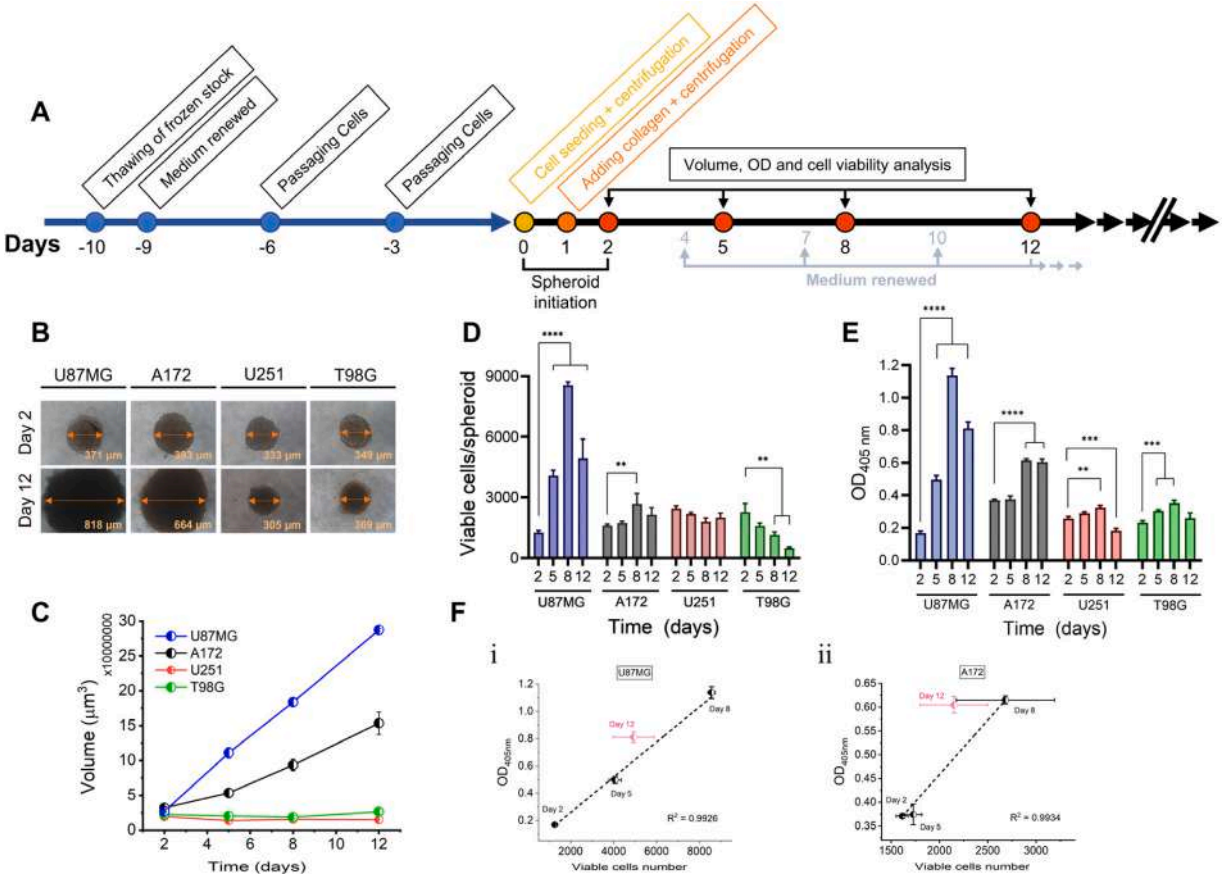

Fig. 1. Characterization of U87MG, A172, U251, and T98G spheroids as a function of time from day 2 to 12 at an initial cell density of 2000 cell/spheroid. (A) timeline of spheroid formation and culture. (B) optical images on day 2 and day 4. (C) volume *versus* time of culture. (D) viability/spheroid by trypan blue assay *versus* time of culture. (E) viability/spheroid by acid phosphatase assay *versus* time of culture acid phosphatase. (F) OD from acid phosphatase *versus* viable cell number by Trypan blue for i) U87MG and ii) A172 spheroids. Data points are mean ± standard deviation for 24 spheroids.

In contrast, the viability of U251 and T98G spheroids started decreasing immediately after day two, especially for T98G. These results indicated a low proliferative process in these spheroids. It is worth noting that, for T98G cells, the relative cell viability strongly decreased, showing that only a minor fraction of cells was viable on day 12.

In addition to trypan blue, an acid phosphatase assay was performed as a second viability assay to confirm the findings and evaluate the correlation between both methods (Fig. 1E). The acid phosphatase assay is a method based on the quantification of cytosolic acid phosphatase activity that hydrolyzes *p*-nitrophenyl phosphate to *p*-nitrophenol, resulting in absorption values at 405 nm proportional to cell number in the range of 10^3 to 10^5 cells in the monolayer. This method determines the viability of single spheroids without any prior disruption. Acid phosphatase exhibited similar behavior for cell viability in U87MG and A172 spheroids compared with the trypan blue assay. Up to day eight, a good correlation was observed between the methods. However, a deviation appeared on day 12 (Fig. 1F). The deviation in acid phosphatase response at longer spheroid cultures has also been observed in previous studies, but the cause was unclear [34]. Here, we show that the formation of a necrotic nucleus might be involved in such a deviation. The deviation between the methods was observed for U251 and T98G cells even after day two (not shown), which resulted in high cell death. To the best of our knowledge, this is the first study to use an acid phosphatase assay to establish a comparison between the most common GBM spheroids and cell counting. The linear correlations between viable cell number and acid phosphatase OD can assist researchers in

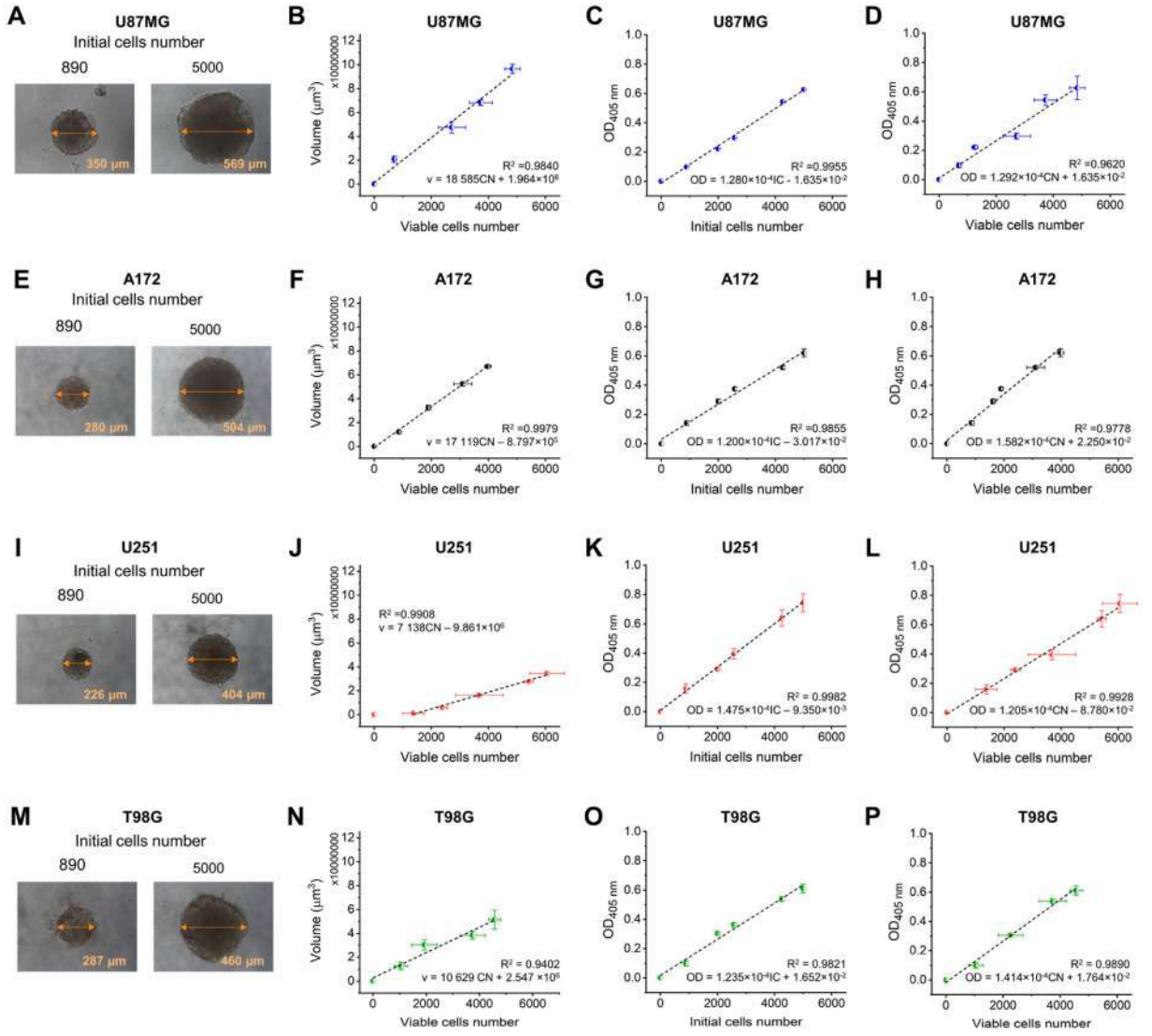

Fig. 2. U87MG, A172, U251, and T98G spheroids on day 2 at different seeding densities. Optical images for initial cell numbers being 890 and 5000 on day 2 for (A) U87MG, (E) A172, (I) U251, and (M) T98G. Volume *versus* time of culture viable cell number by trypan blue for (B) U87MG, (F) A172, (J) U251, and (N) T98G cells. OD from acid phosphatase *versus* the initial cell number for (C) U87MG, (G) A172, K) U251, and O) T98G. OD from acid phosphatase *versus* viable cell number by trypan blue for (D) U87MG, (H) A172, (L) U251, and (P) T98G cells. Data points represent the mean ± standard deviation for 24 spheroids.

viability assays and drug screening using GBM spheroids.

After describing the effect of time on spheroid properties, we aimed to study how the initial cell number affects the properties of the GBM spheroids. The assays were conducted on day two of incubation to avoid any effects on the necrotic nucleus. Optical microscopy images are presented in Fig. 2A (U87MG), 2E (A172), 2I (U251), and 2M (T98G) formed by 890 and 5000 cells, respectively. We found that the spheroid diameter increased as the initial cell number increased, with a good correlation between volume and initial cell number (Fig. 2B, F, J, and N). Cell compaction was in the following order: U87MG < A172 < T98G < U251. These results suggest a correlation between cell compaction and cell death, except for U251. In this case, the highest compaction of the U251 spheroids might be related to strong cell-to-cell interactions that cause significant compaction without collagen. The absence of type I collagen might also contribute to higher compaction.

Acid phosphatase OD signal correlated well with the initial (Fig. 2C, G, K, and O) and viable (Fig. 2D, H, L, and P) cell numbers, indicating the absence of necrotic nucleus formation on day 2. This was true even for the highest U87MG spheroid [569 (±8) μm in diameter] formed by 5000 cells. It is worth noting that this diameter is above the limit that caused necrotic nuclei with time, as described earlier. Interestingly, A172 spheroids presented the lowest viable cell number among spheroids, even when compared with T98G cells, which presented an intense cell death process over time. Once all cell lines studied present similar doubling times according to literature [35–37], the proliferative effect seems not to be the main factor driving the viability data observed. Thus, some cell death processes were significantly present in the A172 spheroids. This finding explains the lower number of A172 viable cells on day 5 compared with U87MG. The differences in the value of the angular coefficient of the linear relationship between OD and cell number from Trypan blue showed that the OD of phosphatase acid depends on the number of cells and the cell/spheroid characteristics. For the next experiments, we selected days 4 and 12 since day 4 presented high cell proliferation with uniform morphology and day 12 was the final period analyzed.

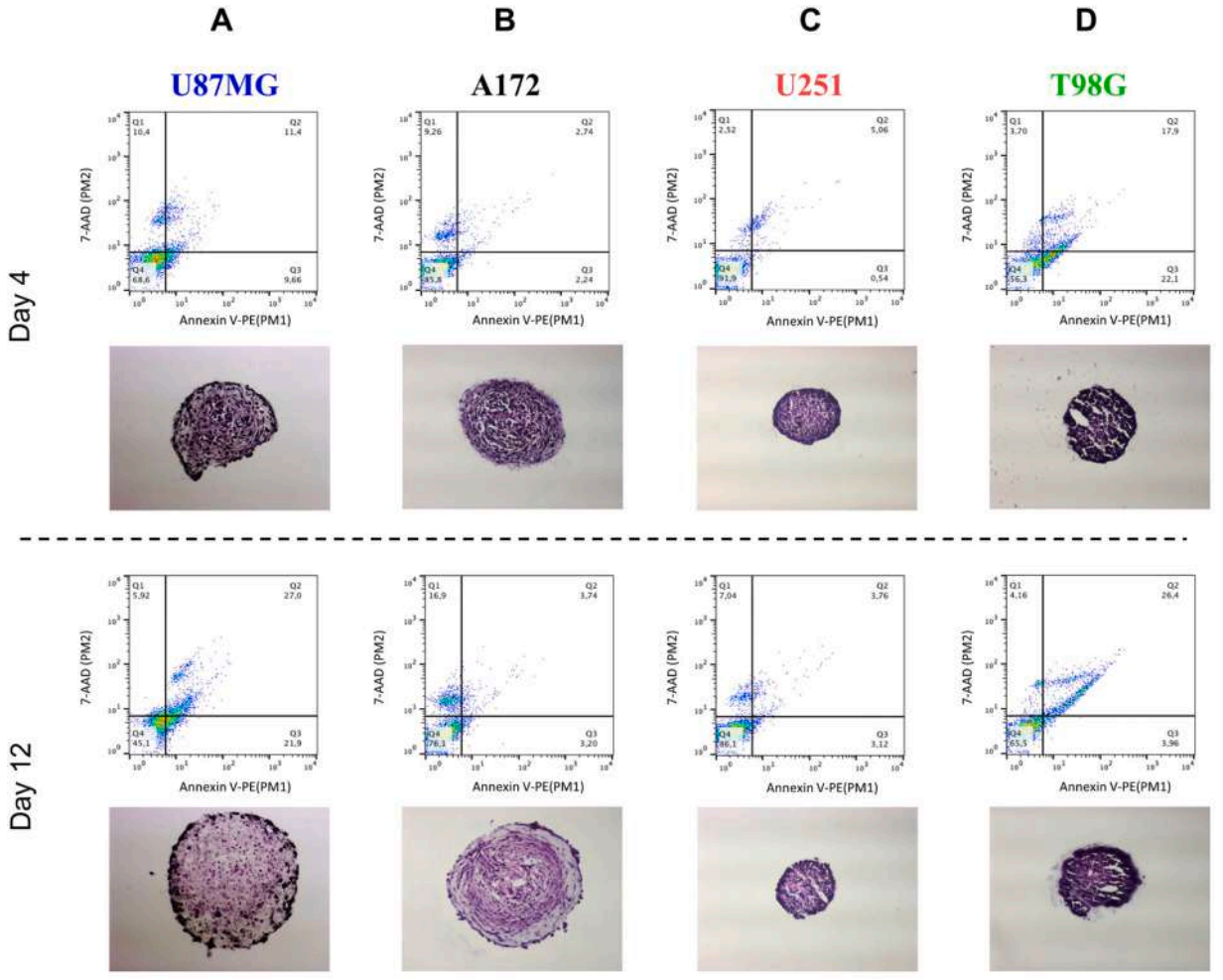

Fig. 3. Annexin V / 7-AAD analysis by flow cytometry (5×10^4 events/sample) and representative microscopic images of hematoxylin/eosin (H&E)-stained for GBM spheroids (A) U87MG, (B) A172, (C) U251, and (D) T98G on days 4 and 12.

3.2. Analysis of cell death and histology

To expand the findings on the cell death processes in our GBM spheroids, we analyzed the stages of cell death using flow cytometry with annexin V/7-AAD staining. The results are illustrated in Fig. 3. Quadrant 4 (Q4) denotes vital cells (both Annexin V and 7-AAD negative), while Q3 corresponds to early apoptosis (Annexin V-positive and 7-AAD-negative populations). Late apoptosis (Annexin V and 7-AAD positive) is represented in Q2 and Q1 related to necrosis (Annexin V-negative and 7-AAD positive).

In U87MG cells (Fig. 3A), necrosis was observed on day 4 and the percentage of apoptotic cells significantly increased from day 4 to day 12. Necrosis plays a role in stimulating apoptosis. Inducible apoptosis does not occur independently of necrosis [38]. Histology using hematoxylin and eosin (H&E) assay of cryosectioned spheroids showed high cell viability along the spheroid on day 4 but decreased viable cells in the nucleus region on day 12.

Together, these results demonstrated the formation of necrotic nuclei over time. Notably, the higher cell viability on the edge of spheroids on day 12 agreed with the spheroid growth over time. In the case of A172 cells (Fig. 3B), flow cytometry demonstrated that cell death was more related to necrosis in U87MG cells, agreeing with cell viability in Fig. 1. H&E staining showed fewer viable cells in the nucleus on day 12, but the spheroid organization was preserved. Viable cells on spheroid edges on day 12 ensured interfacial cell proliferation.

In the case of U251 cells (Fig. 3C), cell viability was stable over time. This corroborates the approximately unchanged viability shown in Fig. 1C and D. The H&E images showed modest tissue differences with time, with an increased disorder on day 12. The T98G spheroids (Fig. 3D) showed significant late apoptosis on day 4, with a further increase on day 12. H&E staining showed a highly disordered tissue even on day 4, which is typical of spheroids with low viability. These results are consistent with the early decrease in the viability of T98G cells over time in Fig. 1D. The results revealed that U251 spheroids are viable up to day 12, in contrast to T98G spheroids, which are prone to cell death.

In summary, the results demonstrated that GBM spheroids increase cell death with a higher terminal stage of cell death, necrosis, and early apoptosis. Hematoxylin and eosin (H&E) assays indicated essentially higher cell death at the center than at the interface of spheroids over time. The U87MG and A172 spheroids maintained a structure organized for the tissue over time, supporting an increase in viability during the first days of growth. U251 cells showed lesser changes with time, even in size, proliferation, or cell death-related events. T98G spheroids showed high cell death processes with a less organized tissue, as showed by H&E stain. These findings showed that GBM spheroids have unique structures and characteristics according to the cell line, which evaluated nanoparticle's uptake and application in PDT in such spheroids.

3.3. Uptake and cytotoxicity of AlClPc-loaded liposomes

Solid tumors have high extracellular matrix (ECM) content that drug delivery systems must overcome to enter and pass through the core. ECM components may prevent convective flow within the tumor matrix, limiting the rate of movement of molecules and nanomaterials through the tumor tissue via diffusion [39]. In this scenario, type-I collagen plays a crucial role in the ECM of GBM, directly affecting the patient survival [40]. The GBM spheroids used in this study contained type-I collagen as an ECM for compaction, which makes our spheroids good 3D models in nanomedicine for testing the penetrability of liposomes in the early stages of drug development.

First, we evaluated the cellular uptake and penetration range of AlClPc-loaded liposomes (H_D equal to 104.2 nm and PdI = 0.209) in U87MG spheroids (Fig. 4). U87MG was chosen as the standard spheroid model to ensure the accuracy and reliability of the experiment because of its larger diameter and higher cell viability on day 4.

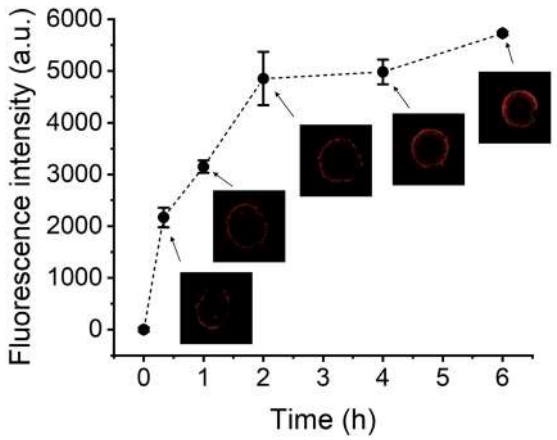

Fig. 4. Cell uptake of Lip-Pc (10 μmol L^{-1}) in U87MG (2000 cells/spheroid, day 4) spheroids as a function of time. Measurements by fluorescence intensity with excitation at 630 nm and fluorescence at 672 nm. Inside are confocal microscopy images of serial sections of GBM spheroids. Data points are mean ± standard deviation for 21 spheroids.

For the Lip-Pc penetration range analysis, spheroids were fixed, serially cut using a cryostat, and imaged using a confocal laser microscope with a filter for phthalocyanine at 630 nm (Fig. 3). The histological section avoids artifacts such as limited laser penetration into the core of the integral spheroids [17]. The results demonstrated that Lip-Pc uptake was time-dependent. After 20 min, a week fluorescence was observed on the outer part of the spheroid. The border of the spheroids was filled with Pc after 1 h. Increasing the time increased the color intensity. A number of cells took up the drug center of the spheroid after 4 h incubation. By measuring the total area of spheroids and the area taken by the fluorescence of Pc, we found approximately 47% of the spheroid area contained Lip-Pc fluorescence at 4 h, increasing it to 55% of the area at 6 h. Although the uptake of nanoparticles is strongly influenced by the size, nature of the material, and charge of particles [39], GBM spheroids allow drug penetration even in the presence of ECM components, confirming that such GBM spheroids help study nanomedicine uptake as a mimic model of solid tumors.

The successful results of Lip-Pc uptake in GBM spheroids motivated us to carry out PDT cytotoxicity studies. The cytotoxicity of Lip and Lip-Pc in the absence of light was assessed using an acid phosphatase assay in U87MG spheroids (Fig. S1). None of the formulations was cytotoxic to the U87MG spheroid model after 4h of incubation. At 10 μmol L^{-1} of AlClPc (for Lip-Pc), the cell viability was approximately 90 ± 3%. In contrast, previous studies using 2D monolayer cells of U87MG treated with 10 μmol L^{-1} of AlClPc-loaded nanoemulsion showed a 24 ± 3% cell viability [41], a value much lower than that presented in the 3D culture. The findings demonstrate that the use of 3D models is fundamental in drug discovery studies and new therapies because the cytotoxicity of formulations in 3D spheroids is closer to that of *in vivo* models than in the 2D approach.

3.4. GBM spheroids as a tumor model for photodynamic therapy

Encouraged by the outstanding low cell cytotoxicity of Lip-Pc in U87MG spheroids, we tested phototoxicity in GBM spheroids as a tumor non-animal model for PDT assays. We chose spheroids of the initial 2000 cells per spheroid on day 4 for application in PDT, aiming at high-health spheroids with significant tight compaction and sphericity. Moreover, PDT in spheroids faces issues with oxygen access in the inner parts of the spheroids as their size increases. Therefore, we used spheroids on day 4 to minimize the effects of hypoxia.

Spheroids of U87MG, A172, U251, and T98G cell lines were treated with Lip-Pc (10 μmol L^{-1} AlClPc) for 4 h and LED light (660

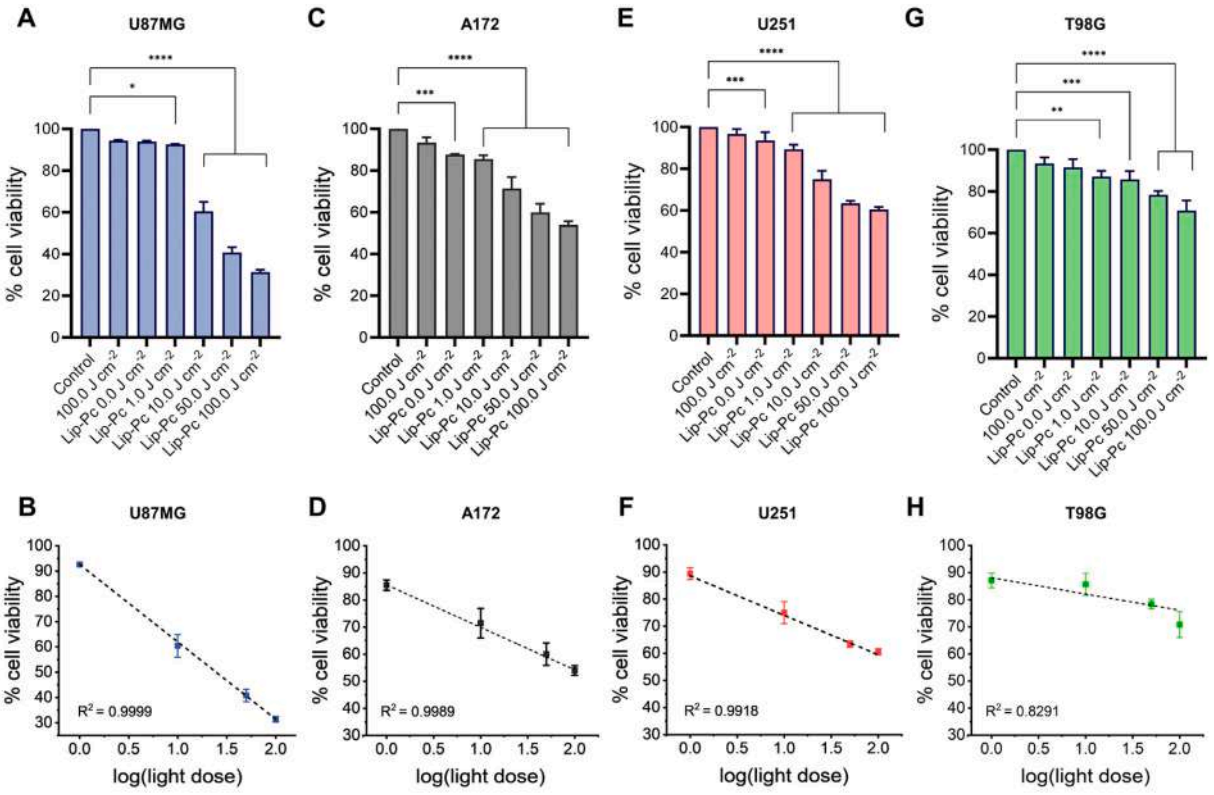

Fig. 5. Cell viability of GBM spheroids (2000 cells/spheroid, day 4) by acid phosphatase assay. (A) U87MG, (C) A172, (E) U251, and (G) T98G. The groups were: cells (Control), cells and laser 100 J/cm^2 (D4), cells treated with free Lip, cells treated with Lip-Pc (10 μmol L^{-1}) submitted to laser (Light Doses used: 0, 1, 10, 50, and 100 J cm^{-2}). Cell viability (%) versus Log(Light Dose) for (B) U87MG, (D) A172, (F) U251, and (G) T98G. Data are reported as the mean of at least three independent triplicate experiments ± standard deviation. *$p < 0.05$, **$p < 0.01$, and *** $p < 0.001$ vs controls (Tukey's test).

nm) was applied at 30 mW/cm^2 for 0.56 min (1 J/cm^2), 5.56 min (10 J/cm^2), 27.78 min (50 J/cm^2), and 55.56 min (100 J/cm^2). Fig. 5 illustrates spheroid cell viability after treatment. No significant decrease in cell viability (> 90%) was observed for control of light dose. Similarly, the Lip and Lip-Pc showed low cytotoxicity in the dark. Conversely, cell viability significantly decreased as a function of light dose in all cell lines evaluated. At 100 J cm^{-2}, cell viability was approximately 31 (±2), 56 (±1), 55 (±1), and 66 (±3)%, respectively, for U87MG, A172, U251, and T98G. It is worth noting that the effective light dose for 2D monolayers is below 1.0 J cm^{-2} using AlClPc at 1.0 μmol L^{-1} in U87MG [42,43]. In contrast, *in vivo* studies used doses higher than 100 J cm^{-2} [22]. Thus, the proximity of the effective light dose used here against GBM spheroids with the *in vivo* dose response in the literature is a proof-of-concept of its applicability as a pre-clinical testing platform to decrease the use of animals in research.

A linear correlation between the logarithm of the light dose used and cell viability results suggested the first-order mechanism of cell death for all cell lines studied. The R^2 values for U87MG, A172, and U251 spheroids were above 0.99, confirming that the excellent linear correlation obtained; the poorest R^2 value for T98G cells might result from its low initial cell viability, which reduces the signal-to-noise ratio. Evaluation of U87MG spheroids showed the lowest cell viability at each light dose applied. Cell viability appeared to have an inverse relationship with compaction. This result might indicate a correlation between tight compaction and resistance to PDT, possibly because of the lower penetration of the drug and molecular oxygen towards the core of the spheroids; such assumption needs further experimental validation. Simultaneously, T98G was the most resistant cell line (highest cell viability) and U87MG demonstrated the best response to Pc photoactivity. One characteristic of GBM is the heterogeneous coexistence of high ROS levels and the overproduction of antioxidant enzymes that can antagonize ROS-based therapies, such as PDT. It is also known that T98G shows high levels of antioxidant enzymes and, consequently, is more resistant to PDT [44]. Other studies suggested a better performance of PDT in 2D models of U87MG than the U251 and T98G cells, probably through the activation of caspase-3 as a critical mediator of apoptosis, which is less pronounced in other cells.

4. Conclusion

We characterized U87MG, A172, T98G, and U251 spheroid models cultured for up to 12 days according to their size, cell viability pathway, histology, cell uptake, and response to PDT. U87MG and A172 spheroids growth in a time-dependent manner for up to 12 days. Compared with other cell lines, the larger size associated with the high viability of U87MG spheroids assures its potential as a standard option for drug screening assays against GBM. A period of eight days was defined as the upper boundary in studies of cell viability for both A172 and U87MG. This is typically due to the formation of necrotic nuclei and loss of organization. T98G and U251 spheroids present low cell viability and growth over time, requiring careful drug screening assays. Under phototherapy using PDT mediated by AlClPc-loaded liposomes, GBM spheroids were more resistant and mimicked the cell response better *in vivo* than 2D monolayers.

Author agreement

The manuscript submitted represents original work and has not been previously published or simultaneously submitted elsewhere for publication. The authors declare that they have no known competing financial interests or personal relationships that could have appeared to influence the work reported in this paper.

Funding sources

We thank the Brazilian Federal Agency for Support and Evaluation of Graduate Education (CAPES), the São Paulo Research Foundation (FAPESP) thematic project #2013/50181-1, FINEP project 01.10.0758.01, and PRONON-SIPAR project #25000.077093/2015-86. We also thank National Council for Scientific and Technological Development (CNPq) for the grant #404416/2021-7, #304687/2021-9 and CNPq-SCTIE-Decit-DGITIS-CGCIS nº 26/2020 – Innovative Platforms in Advanced Therapies #441673/2020-1, PRPI-USP PIPAE Project Agreement #21.1.10424.1.9 and USP-COFECUB Project Agreement #22.1.538.59.4 for their financial support. We also thank Cynthia Maria de Campos Prado Manso for the English language revision and editing. IRC is a recipient of a FAPESP Post-Doc fellowship (#2020/04507-6). SRA receives financial support from CNPq (381476/2020-0).

CRediT authorship contribution statement

Samara Rodrigues Alves: Methodology, Investigation, Formal analysis, Writing – original draft. **Italo Rodrigo Calori:** Methodology, Investigation, Formal analysis, Writing – original draft. **Hong Bi:** Supervision, Visualization, Writing – review & editing. **Antonio Claudio Tedesco:** Conceptualization, Supervision, Visualization, Formal analysis, Writing – review & editing, Funding acquisition.

Declaration of Competing Interest

The authors declare that they have no known competing financial interests or personal relationships that could have appeared to influence the work reported in this paper.

References

[1] E.S. Walker, R.A. Roberts, Collaboration and competition: ethics in toxicology, Toxicol. Res. 7 (2018) 576–585.
[2] C. Tang, T. Prueksaritanont, Use of in vivo animal models to assess pharmacokinetic drug-drug interactions, Pharm. Res. 27 (2010) 1772–1787.
[3] S.B. Gorzalczany, A.G. Rodriguez Basso, Strategies to apply 3Rs in preclinical testing, Pharmacol. Res. Perspect. 9 (2021) e00863.
[4] L. Carbone, Estimating mouse and rat use in American laboratories by extrapolation from Animal Welfare Act-regulated species, Sci. Rep. 11 (2021) 1–6.
[5] G.A. Van Norman, Limitations of animal studies for predicting toxicity in clinical trials: is it time to rethink our current approach? JACC Basic Transl. Sci. 4 (2019) 845–854.
[6] J. Bailey, M. Thew, M. Balls, An analysis of the use of animal models in predicting human toxicology and drug safety, Altern. Lab. Anim. 42 (2014) 181–199.
[7] N. Shanks, R. Greek, J. Greek, Are animal models predictive for humans? Philos. Ethics Hum. Med. 4 (2009) 1–20.
[8] H. Dirven, G.E. Vist, S. Bandhakavi, J. Mehta, S.E. Fitch, P. Pound, R. Ram, B. Kincaid, C.H. Leenaars, M. Chen, Performance of preclinical models in predicting drug-induced liver injury in humans: a systematic review, Sci. Rep. 11 (2021) 1–19.
[9] W.M.S. Russell, R.L. Burch, The principles of humane experimental technique, Methuen, 1959.
[10] S. Lorenzetti, G. Aquilina, F. Caloni, E.M. Coccia, P. Cozzini, G. Cruciani, A. Fouassier, A. Gissi, L. Goracci, T. Heinonen, Non animal methodologies (NAMs): research, testing, assessment and applications–ecopa Symposium 2019, ALTEX-Altern. Anim. Exp. 37 (2020) 317–320.
[11] S.M. Corsello, R.T. Nagari, R.D. Spangler, J. Rossen, M. Kocak, J.G. Bryan, R. Humeidi, D. Peck, X. Wu, A.A. Tang, Discovering the anticancer potential of non-oncology drugs by systematic viability profiling, Nat. Cancer 1 (2020) 235–248.
[12] L. Mohammad-Hadi, A.J. MacRobert, M. Loizidou, E. Yaghini, Photodynamic therapy in 3D cancer models and the utilisation of nanodelivery systems, Nanoscale 10 (2018) 1570–1581.
[13] J.L. King, S.R. Benhabbour, Glioblastoma multiforme – a look at the past and a glance at the future, Pharmaceutics 13 (2021) 1053.
[14] N. Grech, T. Dalli, S. Mizzi, L. Meilak, N. Calleja, A. Zrinzo, Rising incidence of glioblastoma multiforme in a well-defined population, Cureus 12 (2020).
[15] P. Fabbro-Peray, S. Zouaoui, A. Darlix, M. Fabbro, J. Pallud, V. Rigau, H. Mathieu-Daude, F. Bessaoud, F. Bauchet, A. Riondel, Association of patterns of care, prognostic factors, and use of radiotherapy–temozolomide therapy with survival in patients with newly diagnosed glioblastoma: a French national population-based study, J. Neurooncol. 142 (2019) 91–101.
[16] J.P. Fisher, D.C. Adamson, Current FDA-approved therapies for high-grade malignant gliomas, Biomedicines 9 (2021) 324.
[17] H. Sivakumar, M. Devarasetty, D.E. Kram, R.E. Strowd, A. Skardal, Multi-cell type glioblastoma tumor spheroids for evaluating sub-population-specific drug response, Front. Bioeng. Biotechnol. 8 (2020), 538663.
[18] K. Turnovcova, D. Marekova, T. Sursal, M. Krupova, R. Gandhi, P. Krupa, R. Kaiser, V. Herynek, D. Netuka, P. Jendelova, Understanding the biological basis of glioblastoma patient-derived spheroids, Anticancer Res. 41 (2021) 1183–1195.
[19] M. Akay, J. Hite, N.G. Avci, Y. Fan, Y. Akay, G. Lu, J.-J. Zhu, Drug screening of human GBM spheroids in brain cancer chip, Sci. Rep. 8 (2018) 1–9.
[20] A. Musah-Eroje, S. Watson, A novel 3D in vitro model of glioblastoma reveals resistance to temozolomide which was potentiated by hypoxia, J. Neurooncol. 142 (2019) 231–240.
[21] I. de Lázaro, P. Sharp, C. Gurcan, A. Ceylan, M. Stylianou, T. Kisby, Y. Chen, S. Vranic, K. Barr, H. Taheri, Deep tissue translocation of graphene oxide sheets in human glioblastoma 3D spheroids and an orthotopic xenograft model, Adv. Ther. 4 (2021), 2000109.
[22] S.R. Alves, I.R. Calori, A.C. Tedesco, Photosensitizer-based metal-organic frameworks for highly effective photodynamic therapy, Mater. Sci. Eng. C 131 (2021), 112514.
[23] T. Kobayashi, M. Nitta, K. Shimizu, T. Saito, S. Tsuzuki, A. Fukui, S. Koriyama, A. Kuwano, T. Komori, K. Masui, Therapeutic options for recurrent glioblastoma – efficacy of talaporfin sodium mediated photodynamic therapy, Pharmaceutics 14 (2022) 353.
[24] L.R. Aguilar, M.L. Vilchez, L.N.M. Sanabria, Targeting glioblastoma stem cells: the first step of photodynamic therapy, Photodiagn. Photodyn. Ther. 36 (2021), 102585.
[25] H.-A. Leroy, L. Guérin, F. Lecomte, G. Baert, A.-S. Vignion, S. Mordon, N. Reyns, Is interstitial photodynamic therapy for brain tumors ready for clinical practice? A systematic review, Photodiagn. Photodyn. Ther. 36 (2021), 102492.
[26] E. Maestri, The 3Rs principle in animal experimentation: a legal review of the state of the art in Europe and the case in Italy, J. BioTech 10 (2021) 9.
[27] D. Shin, L. Nguyen, M.T. Le, D. Ju, J.N. Le, K. Berg, H. Hirschberg, The effects of low irradiance long duration photochemical internalization on glioma spheroids, J. Photodiagn. Photodyn. Ther. 26 (2019) 442–447.
[28] M.C. Bassler, T. Rammler, F. Wackenhut, S. Zur Oven-Krockhaus, I. Secic, R. Ritz, A.J. Meixner, M. Brecht, Accumulation and penetration behavior of hypericin in glioma tumor spheroids studied by fluorescence microscopy and confocal fluorescence lifetime imaging microscopy, J. Anal. Bioanal. Chem. (2022) 1–12.
[29] S.J. Madsen, C.H. Sun, B.J. Tromberg, V. Cristini, N. De Magalhães, H. Hirschberg, Multicell tumor spheroids in photodynamic therapy, J Lasers Surg Med. Off. J. Am. Soc. Laser Med. Surg. 38 (2006) 555–564.
[30] I.R. Calori, S.R. Alves, H. Bi, A.C. Tedesco, Type-I collagen/collagenase modulates the 3D structure and behavior of glioblastoma spheroid models, ACS Appl. Bio Mater. 5 (2022) 723–733.
[31] L. Rittié, Type I Collagen Purification from Rat Tail Tendons, Fibrosis, Springer, 2017, pp. 287–308.
[32] D.P. Ivanov, A.M. Grabowska, M.C. Garnett, High-Throughput Spheroid Screens Using volume, Resazurin Reduction, and Acid Phosphatase Activity, Cell Viability Assays, Springer, 2017, pp. 43–59.
[33] A. Gouda, O.S. Sakr, M. Nasr, O. Sammour, Ethanol injection technique for liposomes formulation: an insight into development, influencing factors, challenges and applications, J. Drug Deliv. Sci. Technol. 61 (2021), 102174.
[34] J. Friedrich, W. Eder, J. Castaneda, M. Doss, E. Huber, R. Ebner, L.A. Kunz-Schughart, A reliable tool to determine cell viability in complex 3-d culture: the acid phosphatase assay, J. Biomol. Screen 12 (2007) 925–937.
[35] L.D. Ke, Y.X. Shi, S.A. Im, X. Chen, W.A. Yung, The relevance of cell proliferation, vascular endothelial growth factor, and basic fibroblast growth factor production to angiogenesis and tumorigenicity in human glioma cell lines, J. Clin. Cancer Res. 6 (2000) 2562–2572.
[36] L. Kiseleva, A. Kartashev, N. Vartanyan, A. Pinevich, M. Samoilovich, A172 and T98G cell lines characteristics, J. Cell Tissue Biol. 10 (2016) 341–348.
[37] Oraiopoulou, M.E.; Tzamali, E.; Tzedakis, G.; Vakis, A.; Papamatheakis, J.; Sakkalis, V.J.B.r.i. In vitro/in silico study on the role of doubling time heterogeneity among primary glioblastoma cell lines, (2017).
[38] H. Bell, I. Whittle, M. Walker, H. Leaver, S. Wharton, The development of necrosis and apoptosis in glioma: experimental findings using spheroid culture systems, Neuropathol. Appl. Neurobiol. 27 (2001) 291–304.
[39] A. Tchoryk, V. Taresco, R.H. Argent, M. Ashford, P.R. Gellert, S. Stolnik, A. Grabowska, M.C. Garnett, Penetration and uptake of nanoparticles in 3D tumor spheroids, Bioconjugate Chem. 30 (2019) 1371–1384.
[40] K.B. Pointer, P.A. Clark, A.B. Schroeder, M.S. Salamat, K.W. Eliceiri, J.S. Kuo, Association of collagen architecture with glioblastoma patient survival, J. Neurosurg. 126 (2016) 1812–1821.
[41] A. Castilho-Fernandes, T.G. Lopes, F.L. Primo, M.R. Pinto, A.C. Tedesco, Photodynamic process induced by chloro-aluminum phthalocyanine nanoemulsion in glioblastoma, Photodiagn. Photodyn. Ther. 19 (2017) 221–228.
[42] M.T. de Melo, H.L. Piva, A.C. Tedesco, Design of new protein drug delivery system (PDDS) with photoactive compounds as a potential application in the treatment of glioblastoma brain cancer, Mater. Sci. Eng. C 110 (2020), 110638.
[43] A.C. Tedesco, E.P. Silva, C.C. Jayme, H.L. Piva, L.P. Franchi, Cholesterol-rich nanoemulsion (LDE) as a novel drug delivery system to diagnose, delineate, and treat human glioblastoma, Mater. Sci. Eng. C 123 (2021), 111984.
[44] M.D. Caverzán, L. Beaugé, C.A. Chesta, R.E. Palacios, L.E. Ibarra, Photodynamic therapy of Glioblastoma cells using doped conjugated polymer nanoparticles: an in vitro comparative study based on redox status, J. Photochem. Photobiol. B 212 (2020), 112045.